Geomechanics and Engineering, *Vol. 9, No. 5 (2015) 645-667*
DOI: http://dx.doi.org/10.12989/gae.2015.9.5.645

Stress field interference of hydraulic fractures in layered formation

Haiyan Zhu [*1], Xudong Zhang [1], Jianchun Guo [1a], Yaqin Xu [2], Li Chen [3], Shuhang Yuan [4], Yonghui Wang [5] and Jingya Huang [1]

[1] *State Key Laboratory of Oil and Gas Reservoir Geology and Exploitation, Southwest Petroleum University, Sichuan, Chengdu, China*
[2] *Safety Environment Quality Surveillance &Inspection Institude, CNPC Chuanqing Drilling Engineering Company Limited, Sichuan Guanghan, China*
[3] *Luming company, Shengli Oil Field, Sinopec, Dongying, China*
[4] *Research Institute of Engineering and Technology, PetroChina Southwest Oil and Gas Fields Company, Sichuan Guanghan, China*
[5] *Research Institute of Petroleum Exploration and Development-Langfang, Petrochina, Langfang, China*

(*Received October 31, 2014, Revised June 03, 2015, Accepted July 14, 2015*)

Abstract. Single treatment and staged treatments in vertical wells are widely applied in sandstone and mudstone thin interbedded (SMTI) reservoir to stimulate the reservoir. The keys and difficulties of stimulating this category of formations are to avoid hydraulic fracture propagating through the interface between shale and sand as well as control the fracture height. In this paper, the cohesive zone method was utilized to build the 3-dimensional fracture dynamic propagation model in shale and sand interbedded formation based on the cohesive damage element. Staged treatments and single treatment were simulated by single fracture propagation model and double fractures propagation model respectively. Study on the changes of fracture vicinity stress field during propagation is to compare and analyze the parameters which influence the interfacial induced stresses between two different fracturing methods. As a result, we can prejudge how difficult it is that the fracture propagates along its height direction. The induced stress increases as the pumping rate increasing and it changes as a parabolic function of the fluid viscosity. The optimized pump rate is 4.8 m^3/min and fluid viscosity is 0.1 Pa·s to avoid the over extending of hydraulic fracture in height direction. The simulation outcomes were applied in the field to optimize the treatment parameters and the staged treatments was suggested to get a better production than single treatment.

Keywords: multilayer stress interference; sandstone and mudstone interbedded reservoir; CZM; induced stress; fracture height control

1. Introduction

The study of fracture propagation characteristic in SMTI is significantly important with the extensive use of hydraulic fracturing. The fracture propagation characteristic at the interface and the stress field of hydraulic fractures in layered formations haven't been clarified yet. The fracture

*Corresponding author, Ph.D., E-mail: zhuhaiyan040129@163.com
[a] Professor, E-mail: guojianchun@vip.163.com

http://www.techno-press.org/?journal=gae&subpage=7 ISSN: 2005-307X (Print), 2092-6219 (Online)

geometry at the interface during the propagation can be divided into two types (Anderson 1981, Warpinski and Teufel 1987, He and Hutchinson 1989, Renshaw and Pollard 1995, Wu *et al*. 2004, Gu and Weng 2010): fracture crosses or terminates at the interface. However, normal fracturing model can't solve the stress mechanics problem during the dynamic propagation of the fracture. Some laboratory experiments of the hydraulic fracturing had been carried out on the basis of non-dimensional similar criteria in order to investigate the fracture initiation and propagation during hydraulic fracturing of highly deviated well (Zhu *et al*. 2014b). Another method that has been used to model the propagation of hydraulic fractures is the Cohesive Zone Method (CZM). Yao *et al*. (2010) modeled a hydraulic fracture by using the pore pressure CZM provided in ABAQUS and closely replicated the results from P3D, PKN and the model developed by Dean *et al*. Taking the layer as pore-elastic medium, considering the fracturing fluid leak-off, CZM combined with pore-elastic damage cohesive element definitely solve the stress mechanics problem during the dynamic propagation of the fracture.

Hydraulically fractured horizontals wells and vertical wells are used increasingly to produce ultralow-permeability reservoir, the magnitude and direction of the stress around the fractured productions wells can be changed as the existence of hydraulic fracture (Saberhosseini *et al*. 2014). Warpinski (Warpinski and Branagan 1989) presented the phenomenon through laboratory experiment and field measurement that stress around the fractured production wells can be changed as the existence of initial fracture. Sneddon (Sneddon 1946, Sneddon and Elliot 1946) derived the formula of stress field around a crack in infinite elastic medium. Based on the study of Sneddon, Palmer (1993) analyzed the induced stress of coal seam gas reservoir caused by initial fracture. Soliman (Soliman *et al*. 2010) analyzed distribution regularities of the induced stress among the fractures in horizontal wells by using analytic method combined with superposition principle. A further cognition of the interference among the fractures and the feasibility of network fracturing could be obtained. Olson (Olson and Wu 2012) and Cheng (2009) studied the same problem with displacement discontinuity method. Shin (Shin and Sharma 2014) simulated multi fractures propagation by using finite element method with cohesive element in ABAQUS. Sensitive analysis were made to study the restrain of the middle fracture.

The research recently mainly focus on the interference of multi vertical fractures in horizontal wells. However, there's little research on the interference of multi vertical fractures in vertical wells. Only soliman obtained the analytical solution of the firstly fractured fracture's induced stress. It was proved that the firstly fractured fracture would surely have influence on the stress field of the upper layer. However, the model was assumed isotropy and can't be applied in multilayer reservoir. During the fracturing of SMTI, fractures can easily cross the interfaces and link up with each other, proppants would go under the interlayers which can't be effectively propped. It's important to get familiar with the variation of fracture morphology and induced stress during the fracturing. In this paper, seepage-stress-damage fluid-solid-coupled model was established, dynamic propagation was simulated through pore-elastic damage cohesive element and the different fracturing mode were compared. Consequently, fracture morphology and induced stress of the stress field in SMTI can be analyzed to guide the optimizing of construction parameters and fracturing mode.

2. Establishment of fracture propagation in SMTI

2.1 Basic theory

2.1.1 The relationship among porosity, permeability coefficient and volumetric strain

During hydraulic fracturing, porosity, permeability coefficient and volume strain interact with each other. This phenomenon is called seepage and stress coupling (Chen *et al*. 2010). The relationship among porosity, permeability coefficient and volumetric strain is

$$k / k_0 = [(\frac{1}{n_0})(1+\varepsilon_V)^3 - (\frac{1-n_0}{n_0})(1+\varepsilon_V)^{-1/3}]^3 \tag{1}$$

Where n_o is the initial porosity, ε_v is the volumetric strain. k is the permeability. k_0 is the initial permeability.

2.1.2 Damage initiation and propagation criterion

The damage pattern of cohesive element follows traction-separation rules.

(1) Cohesive damage initiation criterion

The quadratic interaction function involving the nominal stress ratios equals to one when the damage is about to happen. The criterion could be presented as

$$\left\{\frac{\langle t_n \rangle}{t_n^0}\right\}^2 + \left\{\frac{t_s}{t_s^0}\right\}^2 + \left\{\frac{t_t}{t_t^0}\right\}^2 = 1 \tag{2}$$

Where, t_n, t_s, t_t are the tractions(stresses) in three loading directions (t_n for opening, t_s, t_t for shear direction); t_n^0, t_s^0, t_t^0 are the corresponding prescribed damage initiation tractions (t_n^0 for opening, t_s^0, t_t^0 for shear direction).

(2) Cohesive damage evolution criterion

The damage evolution model describes the rate at which the material stiffness is degraded once the corresponding initiation criterion is reached. The damage evolution is modeled as follow

$$\begin{aligned} t_n &= \begin{cases} (1-D)\bar{t}_n, & \bar{t}_n \ge 0 \\ \bar{t}_n, & \end{cases} \\ t_s &= (1-D)\bar{t}_s \\ t_t &= (1-D)\bar{t}_t \end{aligned} \tag{3}$$

Where, $\bar{t}_n$, $\bar{t}_s$, $\bar{t}_t$ are the stresses in the three loading directions with the assume that the evolution doesn't happen and the model is still in linear elastic deformation process; t_n, t_s, t_t are the real stresses in the three loading directions; D are dimensionless damage coefficient ranges from 0 to 1. If D = 0 the material hasn't damaged yet and if D = 1 the material damaged completely. The Griffith and Irwin's equation is used to calculate the fracture energy

$$G_{IC} = \frac{K_{IC}^2\left(1-v^2\right)}{E} \tag{4}$$

Where G_{IC} is the fracture energy, J; K_{IC} is the fracture toughness, Pa·m$^{0.5}$; v is the Possion's ratio, dimensionless; E is young's modulus, Pa.

The BK fracture criterion is used to take the mixed mode behavior into consideration. This

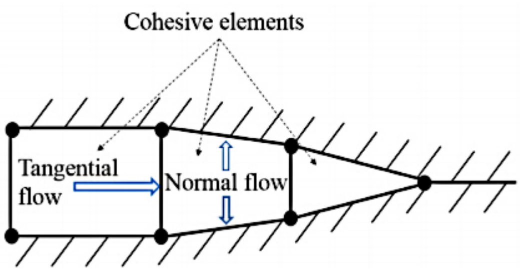

Fig. 1 The sketch map of Fluid flow in the cohesive elements

fracture criterion is particularly useful when the critical energies during deformation purely along the first and the second shear directions are the same.

$$G^c = G_n^c + \left(G_s^c - G_n^c\right)\left\{\frac{G_s + G_t}{G_n + G_s + G_t}\right\}^{\eta} \tag{5}$$

Where G_n^c is the critical fracture energy in mode I,J; G_s^c is the critical fracture energy in mode II,J; G_n is the accrued fracture energy in mode I,J; G_s is the accrued fracture energy in mode II,J; G_t is the accrued fracture energy in mode III,J; η is exponent, dimensionless.

2.1.3 Fluid flow in the fracture

Fluid flow in the cohesive elements along with the normal and tangential direction (Zhu *et al*. 2014a). The tangential flow force the fracture to propagate and the normal flow indicates the fracturing fluid leak-off into the formation (Fig. 1).

The fracturing fluid is assumed as Newton fluid and the fluid leak-off from the fracture into the formation was modeled with the following equations

$$\begin{cases} q_t = c_t\left(p_i - p_t\right) \\ q_b = c_b\left(p_i - p_b\right) \end{cases} \tag{6}$$

Where, q_t, q_b are the velocity of upper and lower surface the fluid leak into the formation; c_t, c_b are leak-off coefficient of the fracture surface; p_i is middle surface pressure of cohesive element; p_t, p_b are pressure of fracture surface. The fluid leak-off coefficients are input as constants or functions of field variables by the user and can be interpreted as the effective permeability of a finite layer on the cohesive element surfaces (Chen *et al*. 1997, Chen *et al*. 2009).

2.2 The finite element model establishment of 408VF well

2.2.1 Model establishment

The northern of Zhuang23 in Shengli is sand-shale interbedded reservoir which has many long and thin layers with different thickness. The reservoir has high temperature and the rock physical property is anisotropic. According to the analysis of the well tests in this area. The porosity is 1.5%~23.6%, 11.49% in average, and the permeability is 0.04349 ~ 25.3508 × 10-3 μm^2, 0.8815 × 10-3 μm^2 in average. From the early oil tests, some wells have some relatively low natural productivity, so fracturing stimulation should be taken to improve the productivity.

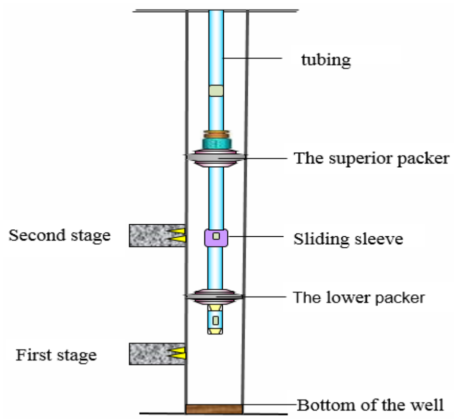

Fig. 2 The schematic of the staged treatments in the vertical well

The staged treatments in vertical well is widely applied in sandstone and mudstone interbedded reservoir to stimulate the reservoir, Fig. 2 is the schematic of the staged treatments in the vertical well. According to the treatment characteristic of stage treatments in vertical well, layer 1 is the first stage and layer 2 is the second stage.

408VF is a vertical well, the well depth ranges from 3847 m to 3917 m, and the structure of the well is complicated. According to the well logging results, the well section have three layers and four interlayers. The lithology of the three layers is sand and the four interlayers is shale. The geometric model of the 408VF well reservoir is established (Fig. 3).

Based on the geometric mode of 408VF well, a 3D plane strain finite element model with length of 80 m, width of 60 m and height of 50 m is established (Fig. 4). The fracture is assumed to be symmetrical about the wellbore, so only half of the fracture is modeled. The model have 54810 nodes, 48654 elements and 1802 cohesive elements in total. The vertical stress is loaded in

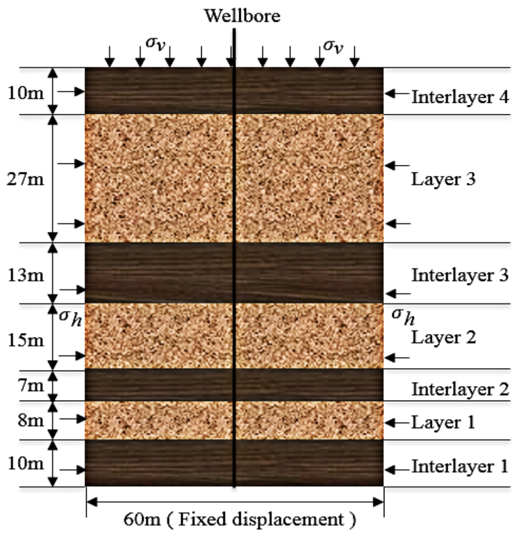

Fig. 3 The geometry model of 408VF well

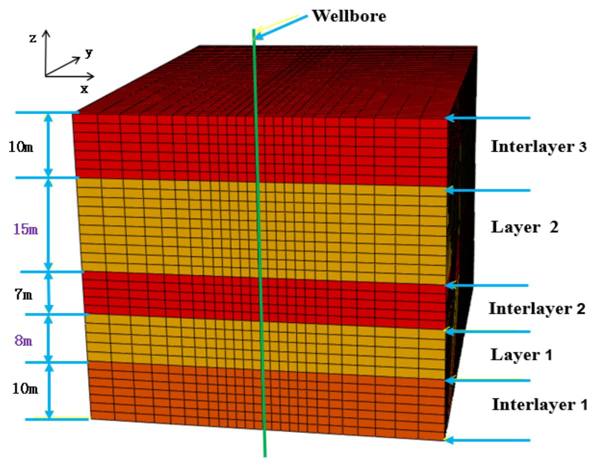

Fig. 4 3D plane strain finite element model

z direction, the minimum horizontal principle stress is loaded in *x* direction, and the maximum horizontal principle stress is loaded in y direction. Wellbore locates in the middle of XZ plane. And the XZ plane is set to the symmetric boundary, the rest boundaries are fixed displacement.

2.2.2 Basic parameters of model

According to the logging results and experiments of rock mechanics, basic parameters of the layers and interlayers (Table 1), basic parameters of cohesive elements (Table 2) and treatment parameters (Table 3) are all shown in the tables.

Table 1 Basic parameters of the layers and interlayers

Position	Lithology	E/GPa	Y	K/ mD	ϕ/%	P_{α}/MPa	σ_v/MPa	σ_H/MPa	σ_h/MPa
Interlayer3	Shale	13	0.27	0.85	6	39.21	95.42	70	63.12
Layer 2	Sand	17	0.26	10	9	39.21	95.62	64.5	54.58
Interlayer2	Shale	13	0.27	0.85	6	39.21	95.78	69	60.27
Layer1	Sand	17	0.26	10	9	39.21	95.88	65.2	55.49
Interlayer1	Shale	13	0.27	0.85	6	39.21	97.82	69.5	61.21

Table 2 Basic parameters of cohesive elements

Position	t_n^0/MPa	t_s^0/MPa	t_t^0/MPa	G_n^C/Pa•m	G_s^C/Pa•m	G_t^C/Pa•m	En/GPa	Es/GPa	Et/GPa
Layer	1	1	1	26.7	26.7	26.7	1830	1830	1830
Interlayer	2	2	2	54	54	54	1830	1830	1830

Table 3 Treatment parameters

Position	C_n/m^3/s	C_t/m^3/s	Injection liquid viscosity/Pa·s	Pumping rate/m^3/s
Layer	5×10^{-6}	5×10^{-6}	0.01	0.05
Interlayer	5×10^{-6}	5×10^{-6}	0.01	0.05

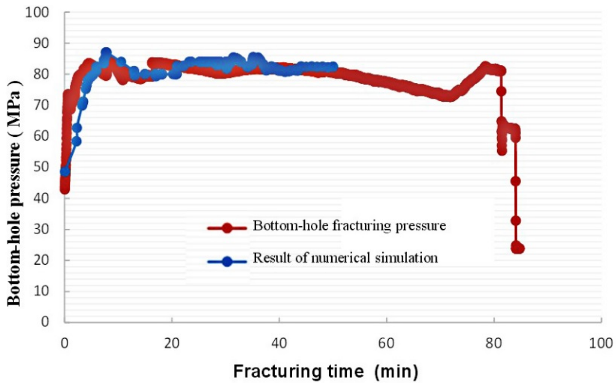

Fig. 5 The comparison of bottom-hole pressure between numerical simulation results and treatments results

2.3 Model verification

The breakdown pressure of the first stage of the well is 63.5 MPa, the extension pressure is 54~57MPa. The stage added proppants 15 m^3 and the sand ratio is 5%~35.6%, the close pressure is 40 MPa. This stage injected prepad fluid 90.6 m3, transport fluid 85.4 m^3 and displacement fluid 23 m^3. The breakdown pressure of the second stage of the well is 61 MPa. This stage added proppants 15 m^3 and the sand ratio is 5%~35.6%, the close pressure is 40 MPa. This stage injected prepared fluid 100.6 m^3, transport fluid 100.4 m^3 and displacement fluid 23 m^3. Firstly, the pressure coming from numerical simulation is compared with the bottom hole fracturing pressure (Zhu *et al*. 2013)

$$P_b = P_s + P_h - P_{pf} - P_f \tag{7}$$

Where: P_b is bottom hole fracturing pressure; P_s is wellhead pumping pressure; P_{pf} is perforation friction; P_f is friction loss along the path; P_h is hydrostatic pressure.

The error between the treatments results and numerical simulation results is below 5% which is within the margin of error (Fig. 5). The 3D model can predict the formation breakdown pressure and the fracture propagation pressure accurately.

3. Result and discussion

3.1 Stress field interference of single fracture

3.1.1 Stress field of the formation

Assuming that staged treatments were firstly constructed in layer 1 and formed a single fracture. The induced stress in the direction of both minimum and maximum horizontal principle stress in interlayer 2 and layer 2 was analyzed. Sensitive analysis was made about the factors affecting the induced stress at the interface. And then the extent and magnitude of the stress interference around the fracture, especially the fracture tip was analyzed. Consequently, whether fracture will cross the interface and link up with each other or not can be discussed in detail. Tensile stress is defined as positive and compression stress is defined as negative in Abaqus.

Beginning with the increasing of treatment time, the fracture extended simultaneously in the

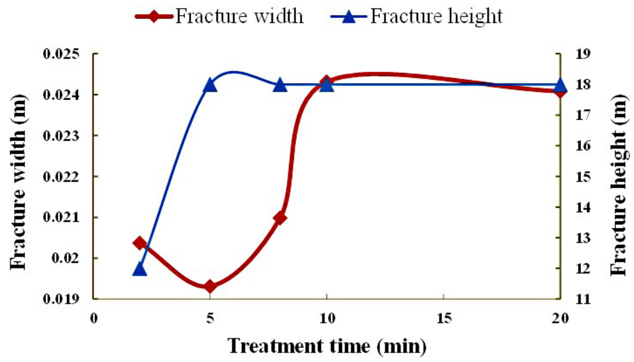

Fig. 6 The variation of fracture height and width with the change of treatment time

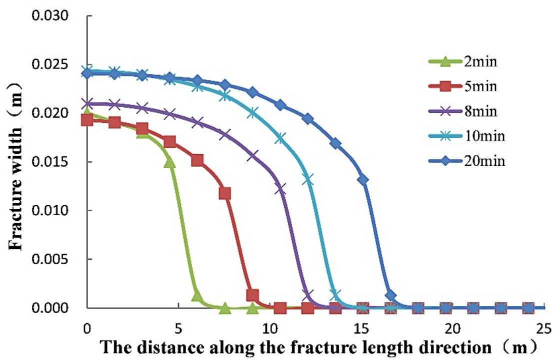

Fig. 7 The variation of fracture length with the change of treatment time

direction of fracture length and fracture height, and the fracture propagated into the interlayer 1 and interlayer 2, the fracture width changed a little in the process. The fracture was no longer propagation in the interlayer 1 after fracturing 5 minutes, the fracture width and fracture height did not change any more after fracturing 10 minutes, but the fracture kept extending in the direction of fracture length. The fracture stopped extending and the treatment is completed after fracturing 20 minutes, the fracture length was about 16m at this time (Figs. 6-7).

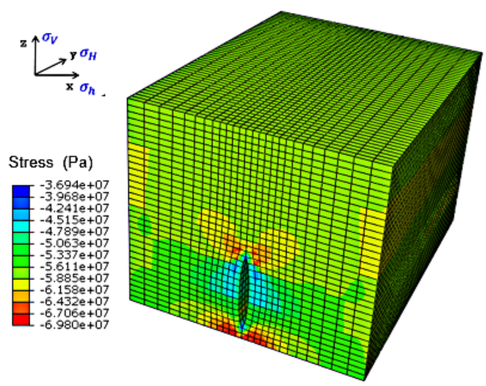

Fig. 8 The contour map of vertical matrix stress

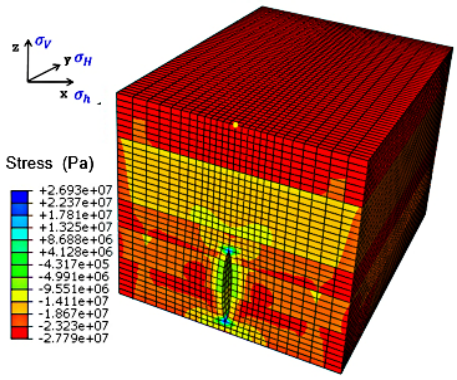

Fig. 9 The contour map of minimum horizontal matrix stress

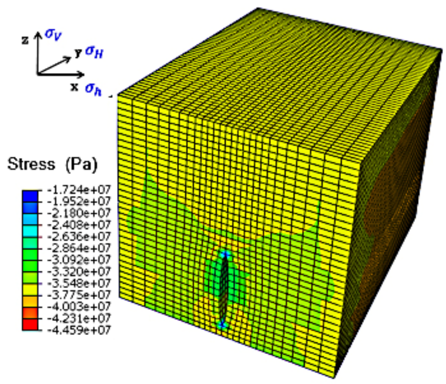

Fig. 10 The contour map of maximum horizontal matrix stress

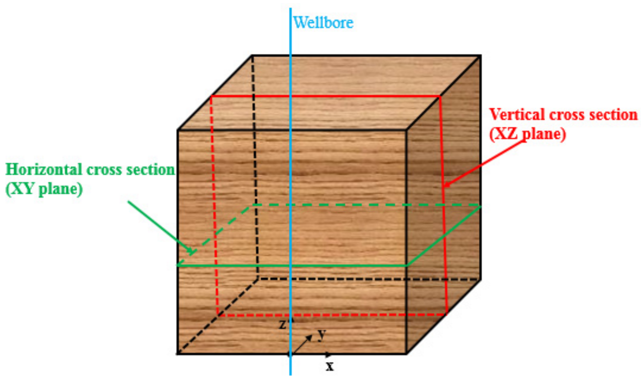

Fig. 11 The sketch map of the section

The vertical matrix stress changes a little, and the matrix stress decreases near the fracture and there is a high compression stress area in front of the tip of the fracture (Fig. 8).

The region near the fracture tips is under compression while it changes into tensile condition after fracturing 20 minutes. There are two high matrix stress regions at both sides of the fracture (Fig. 9). Compared to the contour map of the minimum horizontal matrix stress, the maximum horizontal matrix stress changes a little near the fracture (Fig. 10), and we find that the minimum horizontal matrix stress increases in the region whereas the maximum horizontal matrix stress decreases in the same region, that is to say, the difference of horizontal principle stress reduces. If the sum of the change of the two horizontal principle stress is greater than the original difference of horizontal principle stress, the region will occur stress reversal.

Fig. 11 is the sketch map of vertical and horizontal cross section, the wellbore locates in the vertical plane at $y = 0$ m.

Fig. 12 is the minimum horizontal principle stress direction distribution schematic in the vertical cross section at $y = 0$ m, 6 m, 12 m after fracturing 20 minutes. Red lines represent the direction of minimum horizontal principle stress. The original minimum horizontal principle stress is along the X direction. There are obvious stress interference near the fracture, the extent and angle of stress reorientation near the fracture tips is the largest and then gradually restores to the original direction of minimum horizontal principle stress where far away from the fracture tips. Reorientation distance and the stress reorientation area is shown in the picture. The height and width of fracture decrease with the increasing of the distance along the Y-axis, the extent and the angle of stress reorientation decrease gradually.

Fig. 13 is the minimum horizontal principle stress direction distribution schematic in the horizontal cross section at $z = 8$ m, 13 m, 18 m after fracturing 20 minutes. The region of fracture tips have obvious stress interference, the extent and the angle of stress reorientation is the largest near the fracture tips and then gradually restored to the original direction of minimum horizontal principle stress where far away to the fracture tips. Reorientation distance and the stress reorentation

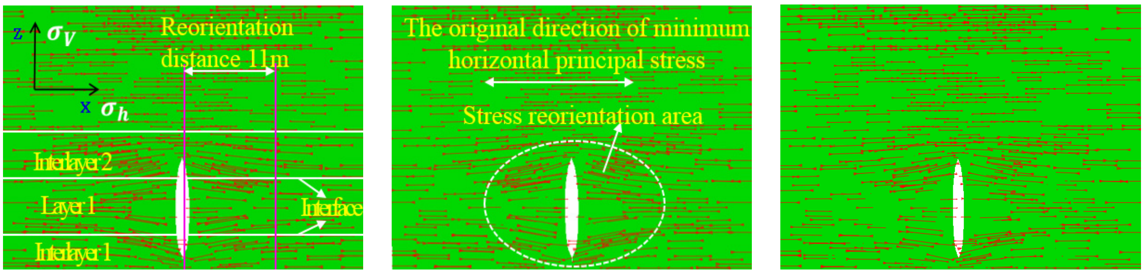

(a) Vertical cross section at $y = 0$ m (b) Vertical cross section at $y = 6$ m (c) Vertical cross section at $y = 12$ m

Fig. 12 Minimum horizontal principle stress direction distribution schematic in vertical cross section

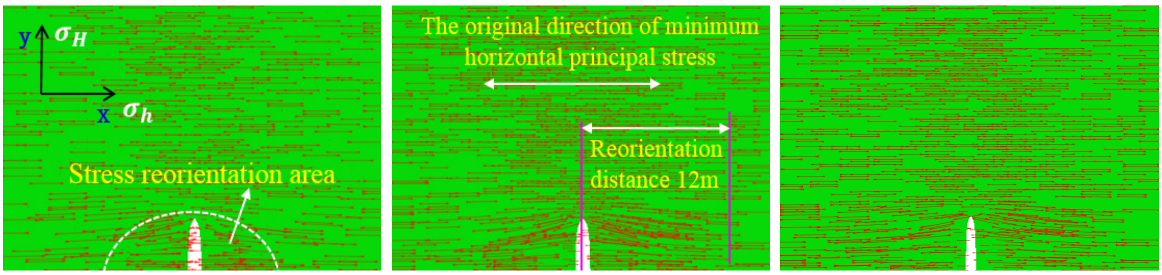

(a) Horizontal cross section at $z = 8$ m (b) Horizontal cross section at $z = 13$ m (c) Horizontal cross section at $z = 18$ m

Fig. 13 Minimum horizontal principle stress direction distribution schematic in horizontal cross section reorientation area is shown in the picture. When the value of z is larger than 18 m, the extent and angle of stress reorientation changes a little, which can be ignored. So the stress interference caused by the fracture 1 extension transfer to interlayer 2 and terminate in it.

3.1.2 Induced stress distribution

The change of the fracture geometry and the pore pressure will results in the change of the original stress condition, the change of the matrix stress is called "induced stress". The induced stress structure is generalized for the case of fractures of arbitrary length and height which allows to describe stress evolution in the process of fracture growth. The new induced stress is defined as follows

$$\begin{cases} \Delta\overline{\sigma}_{\min} = (-\overline{\sigma}_{\min}) - (-\overline{\sigma}_{\min 0}) \\ \Delta\overline{\sigma}_{\max} = (-\overline{\sigma}_{\max}) - (-\overline{\sigma}_{\max 0}) \end{cases} \tag{8}$$

Where: $\Delta\overline{\sigma}_{\min}$, $\Delta\overline{\sigma}_{\max}$ is the induced stress in the direction of minimum and maximum horizontal principle stress MPa ; $\overline{\sigma}_{\min}$, $\overline{\sigma}_{\max}$ is the value of present matrix stress in direction of initial minimum and maximum horizontal principle stress MPa; $\overline{\sigma}_{\min 0}$, $\overline{\sigma}_{\max 0}$ is the value of initial minimum and maximum horizontal matrix stress.

The induced stress in the direction of minimum horizontal principle stress is simplified to "Min induced stress" and the induced stress in the direction of maximum horizontal principle stress is simplified to "Max induced stress".

The value of induced stress denotes the change of the minimum and maximum horizontal stress, at which the positive sign indicates an increase in the stress and the negative sign represents a decrease in the stress. The degree of the compression reduce and makes the fracture propagation much easier.

The minimum and maximum horizontal matrix stress of different plane in layer and interlayer are analyzed, so the Min and Max induced stress under different position of the reservoir can be got and analyzed. The paths and the spacing is defined as what is shown in Fig. 14. The spacing is the vertical distance between the path and the fracture. The origin of coordinates locates in the bottom surface of interlayer 2.

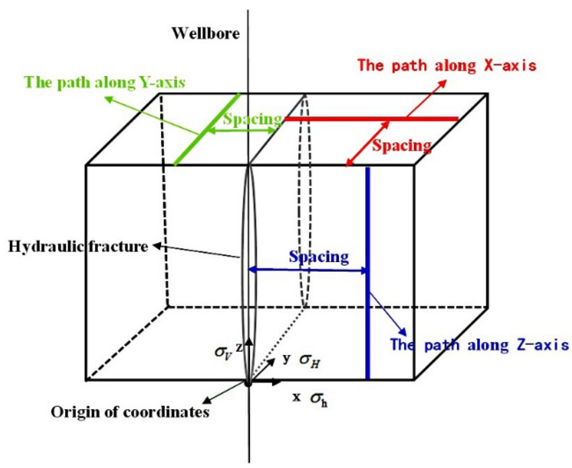

Fig. 14 The sketch map of paths and spacing

3.1.2.1 The stress field of interlayer 2 after fracturing 20 minutes

(1) The variation of induced stress at the paths along the Y-axis direction with different spacing

The paths locate in the top surface of interlayer 2. When the distance along the Y-axis direction is less than 20 m, the Min induced stress alters largely with the increasing of distance and the changing of spacing. The absolute value of Min induced stress decreases gradually with the increasing of spacing and the distance and finally tends to 0.5 MPa (Fig. 15). The absolute value of Max induced stress decrease with the increasing of distance, but increase with the increasing of spacing (Fig. 16). When the distance along the Y-axis direction is more than 20m, the Min and Max induced stress will not change any more. Generally speaking, the impact of induced stress on the top surface of interlayer 2 is small, which can help to prevent further extension in the fracture length direction.

(2) The variation of induced stress at the paths along the X-axis direction with different spacing

The paths locate in the top surface of interlayer 2. The absolute value of Min induced stress increase firstly and then decrease with the increasing of distance along the X-axis direction and finally tends to zero (Fig. 17). The absolute value of Max induced stress changes a little with the increasing of distance along the X-axis direction, but it increases with the increasing of the spacing and finally tends to zero, that is to say, the impact caused by the extension of fracture begin to decrease with the increasing of the spacing (Fig. 18).

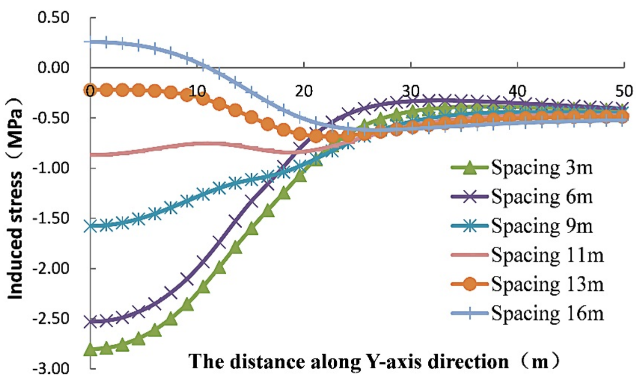

Fig. 15 Variation of Min induced stress with different spacing

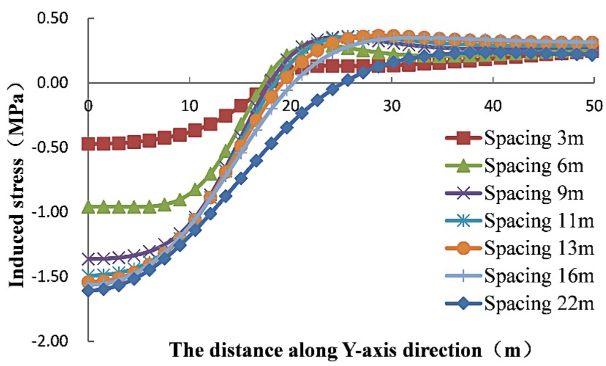

Fig. 16 Variation of Max induced stress with different spacing

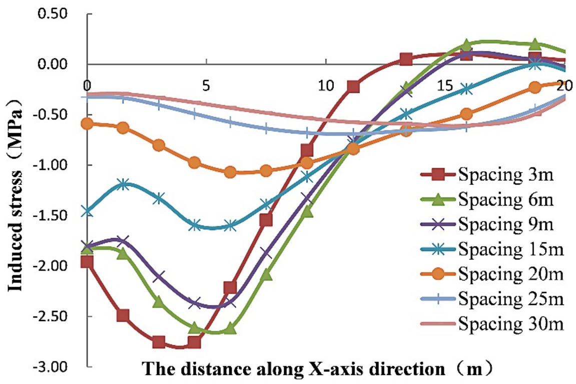

Fig. 17 Variation of Min induced stress with different spacing

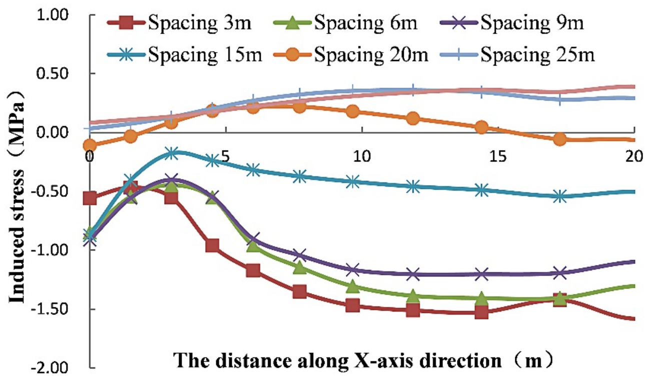

Fig. 18 Variation of Max induced stress with different spacing

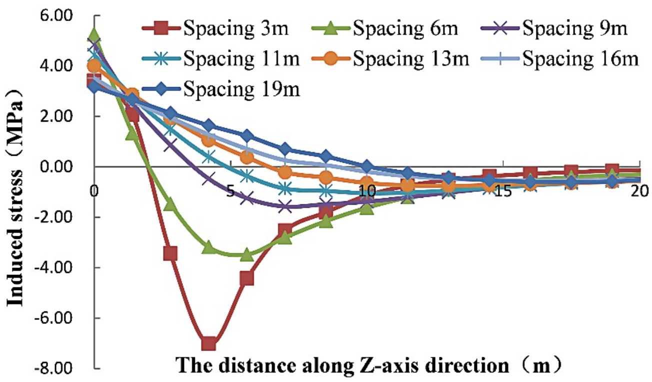

Fig. 19 Variation of Min induced stress with different spacing

3.1.2.2 The stress field of interlayer2 and layer 2 after fracturing 20 minutes

The paths along the Z-axis locate in the vertical cross section at $y = 0$ m. The Min induced stress influenced by the strain in the direction of fracture width is positive at the beginning. The induced stress decrease gradually with the increasing of distance and tends to zero at $z = 12$ m, the thickness of interlayer 2 is 7 m, when the distance along Z-axis direction is over 7 m, the Min induced changes a little, that is to say, the induced stress have small influence on the layer 2 (Fig. 19). The pore pressure-induced stress is dominant in the direction of the maximum horizontal principle stress, so the induced stress is negative. And the absolute value of Max induced stress decrease gradually with the increasing of distance, and it barely change with different spacing (Fig. 20).

3.1.3 Factor analysis for induced stress

The viscosity and pumping rate of fluids affects the fracture geometry, and the change of fracture geometry results in the change of the induced stress around the fracture. The fracture propagated into the interlayer 2 after fracturing 20 minutes, then all nodes on the path 1 at the bottom of layer 2 are selected and could be analyzed (Fig. 21).

3.1.3.1 The effect of treatment parameters on induced stress

(1) The effect of pumping rate on induced stress

The variation of pumping rate result in the change of fracture geometry and the pore pressure. The high pumping rate will decrease the leak off of the injection fluid and increase the net pressure, so the high net pressure results in a greater induced stress. The absolute value of Min and Max induced stress increases with the increasing of pumping rate. The Max induced stress changes a little with the increasing of distance along the X-axis direction (Fig. 23), but the absolute value of Min induced stress increases firstly and then decreases with the increasing of distance and finally tends to zero (Fig. 22). So the low pumping rate helps to control the excessive extension in the direction of fracture height.

(2) The effect of viscosity on induced stress

The viscosity of the fracture fluid affects the width and length profile of the created fracture, in most designs moderate or high viscosity fluids are usually used because of their ability to create sufficient fracture width, and high viscosity can decrease the leak off of the fluid, so the net pressure increase with the increasing of viscosity fluids, so the high viscosity of fluid results in a greater induced stress. The absolute value of Min and Max induced stress decrease with the increasing of viscosity of fluid when the viscosity of injection fluid is less than 0.1 Pa·s and

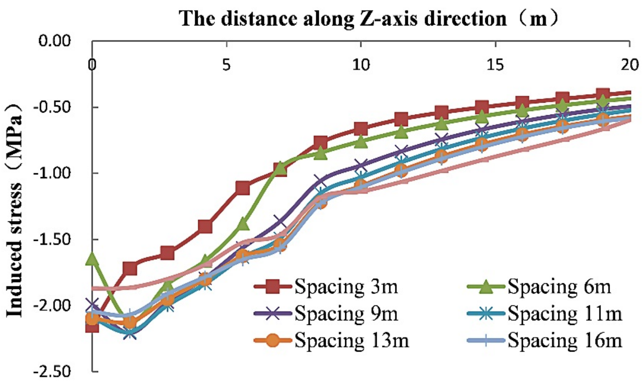

Fig. 20 Variation of Max induced stress with different spacing

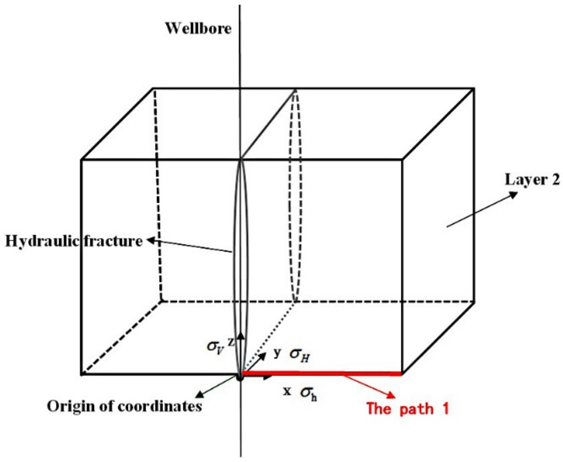

Fig. 21 The sketch map of the path

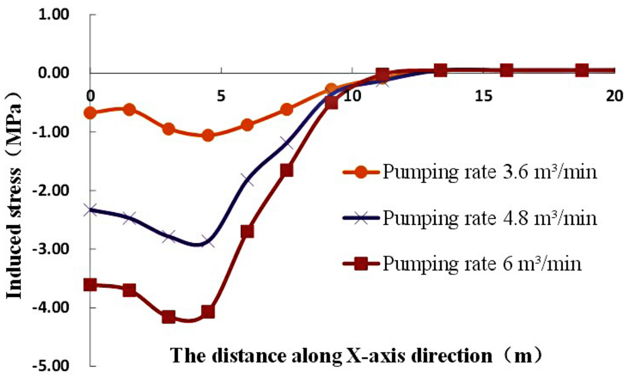

Fig. 22 The variation of Min induced stress with the change of pumping rate

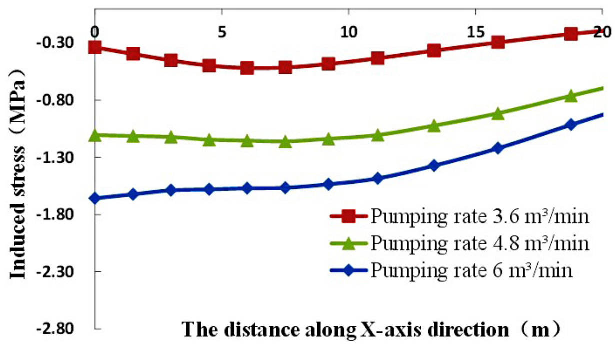

Fig. 23 The variation of Max induced stress with the change of pumping rate

increase with the increasing of viscosity of fracture fluid when the viscosity of fracture fluid is more than 0.1 Pa·s. so the induced stress is minimum when the viscosity of injection fluid is about 0.1 Pa·s. The optimized fluid viscosity is 0.1 Pa·s to avoid the over extending of hydraulic fracture in height direction.

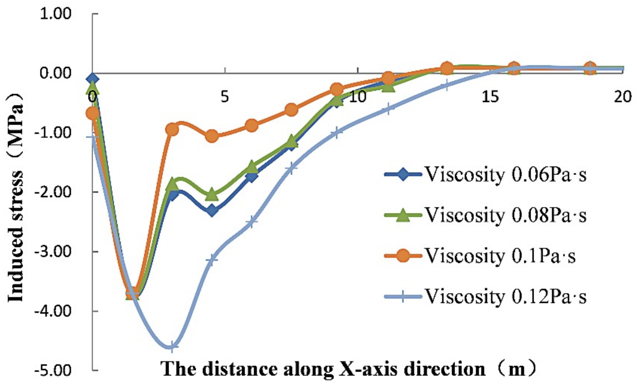

Fig. 24 The variation of Min induced stress with the change of viscosity

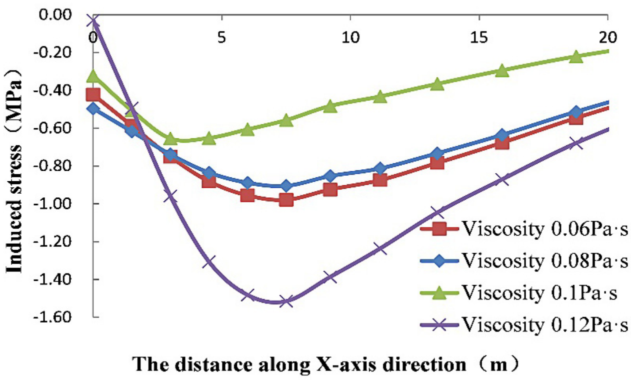

Fig. 25 The variation of Max induced stress with the change of viscosity

3.1.3.2 The effect of the thickness of formation on induced stress

The thickness of layer 1 is 8 m and the thickness of layer 2 is 15 m. The fracture initiates only in layer 1 or layer 2. The variation of induced stress with different thickness of formation at the same fracturing time is analyzed. The paths is defined as what is shown in Fig. 14, The paths along the Y-axis locate in the top surface of the layer 1 or layer 2, three path (spacing 3 m, 6 m, 9 m) cases are studies in this paper.

The thickness of the layer will influence the extension of hydraulic fracture and makes the difference of the fracture geometry. So the fracture initiation in different thickness layer will cause different induced stress, and the induced stress is compared and analyzed. The change trend of Min and Max induced stress keeps the same, but the change amplitude of the induced stress is rather small in the thicker formation. So the Min induced stress have small influence on the interface of the layer when the thickness of reservoir is greater (Fig. 26). So it is hard to extend in the thick formation in the direction of fracture height.

3.2 Stress field interference of double fractures

3.2.1 Stress field of the formation

The fracture 1 initiates in layer 1 and the fracture 2 initiates in layer 2 simultaneously. The fracture 1 propagated into interlayer1 and interlayer 2 and the fracture 2 just extended in layer 2 after fracturing 20 minutes. The region near the fracture 2 tips was under compression while it changed into tensile condition after fracturing 20 minutes (Fig. 27) .The maximum horizontal matrix stress changed a little near the fracture (Fig. 28).

Fig. 29 is the minimum horizontal principle stress direction distribution schematic in the vertical cross section at y = 0 m, 6 m, 12 m after fracturing 20 minutes. Red lines represent the direction of minimum horizontal principle stress. The original minimum horizontal principle

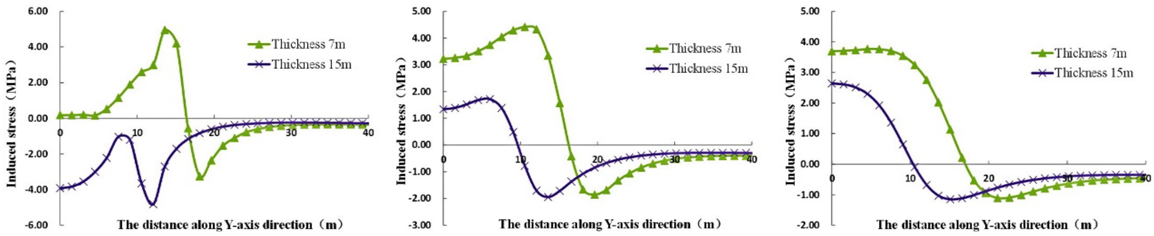

(a) Spacing 3 m (b) Spacing 6 m (c) Spacing 9 m

Fig. 26 The variation of Min induced stress with the change of thickness

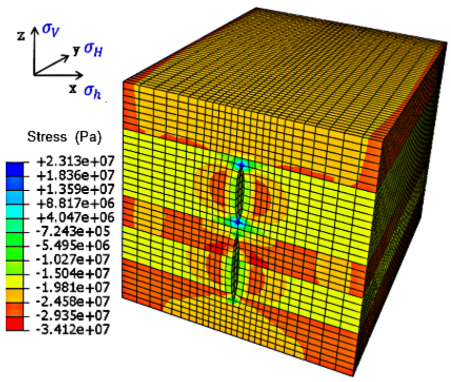

Fig. 27 The contour map of minimum horizontal matrix stress

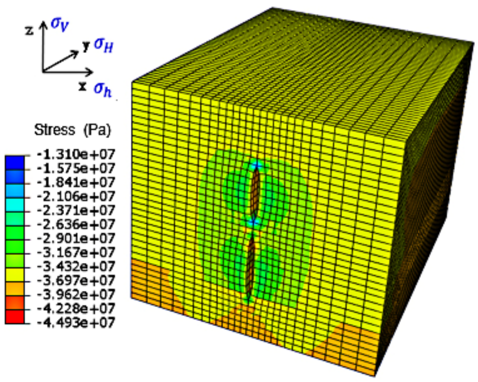

Fig. 28 The contour map of maximum horizontal matrix stress

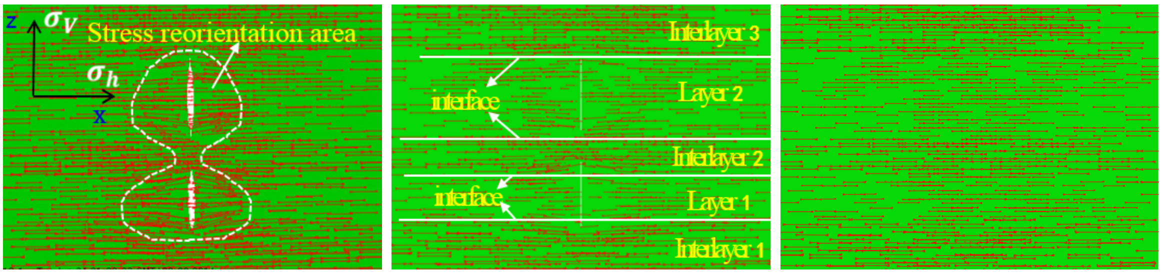

(a) Vertical cross section at $y = 0$ m (b) Vertical cross section at $y = 6$ m (c) Vertical cross section at $y = 12$ m

Fig. 29 Minimum horizontal principle stress direction distribution schematic in vertical cross section

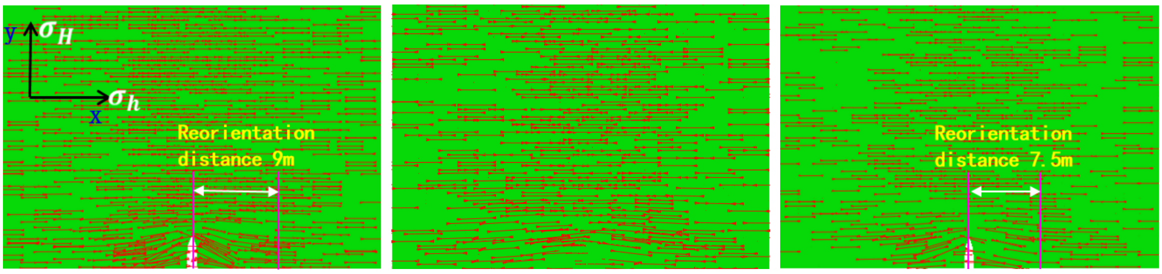

(a) Horizontal cross section at $z = 13$ m (b) Horizontal cross section at $z = 23$ m (c) Horizontal cross section at $z = 33$ m

Fig. 30 Minimum horizontal principle stress direction distribution schematic in horizontal cross section

stress is along the X direction. There are obvious stress interference existing near the fracture especially the fracture tips, so the extent and the angle of stress reorientation near the fracture tips is the largest, and then gradually restores to the original direction of minimum horizontal principle stress where far away from the fracture tips.

Fig. 30 is the minimum horizontal principle stress direction distribution schematic in the horizontal cross section at $z = 13$ m, 23 m, 33 m after fracturing 20 minutes. The region of fracture tips have obvious stress reorientation, and the extent and the angle of stress reorientation is the largest near the fracture tips, and then gradually restores to the original direction of minimum horizontal principle stress where far away to the fracture tips. Reorientation distance and the stress reorientation area is shown in the picture. The induced stress caused by the fracture 1 and fracture 2 have small influence on the interlayer 2 (Horizontal cross section at $z = 23$ m). So the fracture is hard to propagate into the interlayer 3.

3.2.2 Induced stress distribution

The path locates in the top surface of the formation and the spacing is the vertical distance between the path and the fracture. The Min and Max induced stress at the path in layer 1, interlayer 2, and layer 2 is analyzed when just the fracture 1 initiation or double fractures (fracture 1 and fracture 2) initiation simultaneously (Fig. 31).

(1) Stress field of the top surface of layer 1

The induced stress caused by one fracture initiation in the direction of minimum and maximum

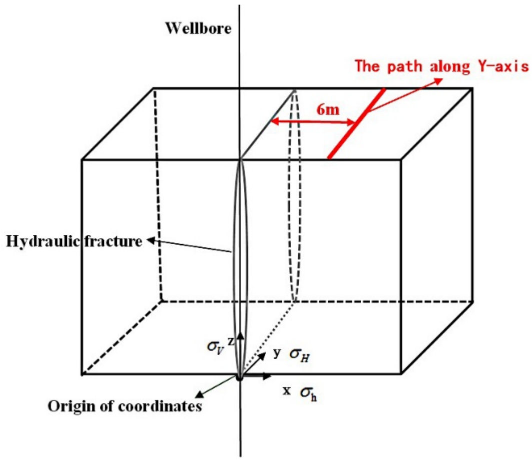

Fig. 31 The sketch map of the path

horizontal principle stress is simplified to “one min” and “one max”, the induced stress caused by two fracture initiation in the direction of minimum and maximum horizontal principle stress is simplified to “two min” and “two max”. The variation of Min and Max induced stress keeps the same under the condition of just the fracture 1 initiation and double fractures initiation simultaneously. But the change amplitude and the trend of double fractures initiation simultaneously is larger than only the fracture 1 initiation. Within a certain distance along the Y-axis direction, the Min induced stress is positive and the Max induced stress is negative, in other words, the maximum horizontal matrix stress decrease and the minimum horizontal matrix stress increase in the same region, if the sum of the change of the two horizontal principle stress is larger than the original difference of horizontal principle stress, the region will occur stress reversal.

(2) Stress field of the top surface of interlayer 2

The change amplitude and trend of double fractures initiation simultaneously is larger than only the fracture 1 initiation. The Min and Max induced stress is negative under the condition of just the fracture 1 initiation. When the distance along Y direction is less than 5 m under the condition of

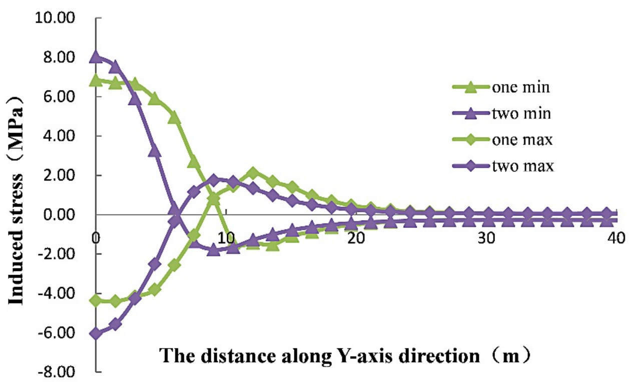

Fig. 32 The variation of induced stress along Y direction

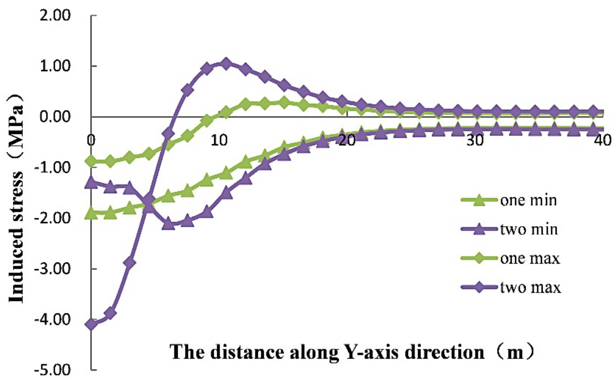

Fig. 33 The variation of induced stress along Y direction

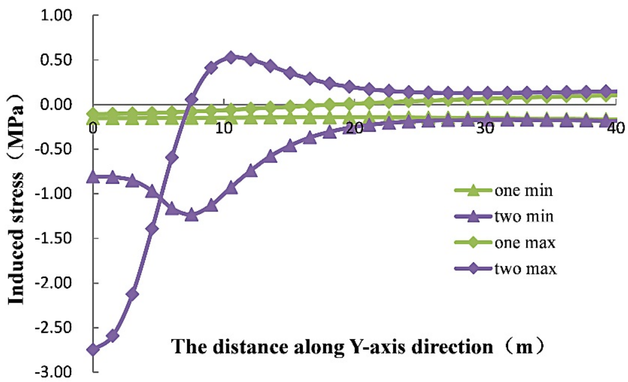

Fig. 34 The variation of induced stress along Y direction

double fractures initiation simultaneously, the variation of Max induced stress is larger than the Min, so if the original difference of horizontal principle stress is small enough, the region will occur stress reversal.

(3) Stress field of the top surface of layer 2

The value of induced stress tends to zero under the condition of just the fracture 1 initiation, so the initiation of fracture 1 have no influence on the top surface of layer 2. When the distance along Y direction is less than 5 m under the condition of double fractures initiation simultaneously, the variation of Max induced stress is larger than the Min, so if the original difference of horizontal principle stress is small enough, the region will occur stress reversal.

4. Field application

There were 29 wells constructed by staged treatments and 7 wells constructed by single treatment. The daily production of single treatment is about 3.4 t. According to the study of this paper, the optimized pumping rate is 4.8 m^3/min and fluid viscosity is 0.1 Pa·s to avoid the over extending of hydraulic fracture in height direction. The simulation outcomes were applied in the field to optimize the treatment parameters and the staged treatments was suggested to get a better

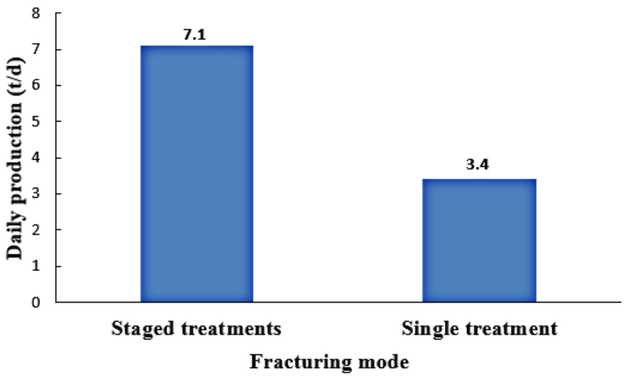

Fig. 35 The comparison of fracturing mode

Table 4 The comparison of treatment parameters

Fracturing mode	Thickness /m	Injection proppants /m^3	The velocity of injection proppants /(m^3/min)	Fracture half-length /m	Production pressure /MPa
Single treatment	23.2	69.1	2.94	159	4
Staged treatments	32.5	120	3.7	166	12.4

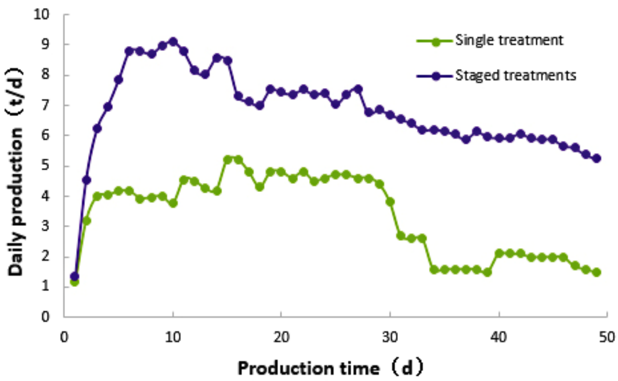

Fig. 36 The variation of production with production time

production than single treatment. The fracture parameters have significantly promoted in staged treatments compared with single treatment (Table 4) which means the stimulation was more thoroughly in plane and vertical direction. All the wells came flowing period after staged treatments and the daily production was larger than the wells constructed by single treatment (Fig. 35).

As is seen, staged fracturing also lowered the production decline rate. The whole reservoir presented the characteristics of “high initial production, low decline rate” and the stimulation effect was significant (Fig. 36). In general, the stimulation effect of staged treatments was better than single treatment. The conclusions of this paper have guided field construction effectively.

5. Conclusions

- 3D model considers the extension of the fracture in the direction of fracture length, and the 3D model can predict the formation breakdown pressure and the fracture propagation pressure accurately. So the 3D model reflects the actual condition of fracture extension in the reservoir accurately.
- The value of the Min and Max induced stress at the interface between interlayer 2 and layer 2 and the interface between layer 2 and interlayer 3 is negative under the condition of double fractures initiate simultaneously, so the matrix stress decreases. Compared to the original state at the interface, the fracture initiate more easily.
- The absolute value of induced stress increases with the increasing of pumping rate and decreases firstly and then increases with the increasing of viscosity of injection fluid, so the induced stress is minimum when the viscosity of injection fluid is about 0.1 Pa·s. The optimized fluid viscosity is 0.1 Pa·s to avoid the over extending of hydraulic fracture in height direction.
- The induced stress caused by the fracture 1 and fracture 2 initiation simultaneously have influence on the interlayer and cause stress reorientation. The change amplitude and trend of double fractures initiation simultaneously is larger than only the fracture 1 initiation. So the fractures are more likely to link up with each other under the condition of double fractures initiation simultaneously.

Acknowledgments

This work was supported by the National Basic Research Program of China (973 Program, No. 2014CB239205). This work was also supported by the PetroChina Innovation Foundation (2014D-5006-0213), the research Foundation of Sichuan Province under Grant No. 2014HH0004, the National Natural Science Foundation of China (No. 51374178) and SWPU academic fund.

References

Anderson, G.D. (1981), "Effects of friction on hydraulic fracture growth near unbonded interfaces in rocks", *Soc. Petrol. Eng. J.*, **21**(1), 21-29.

Chen, Z.X., Chen, M., Jin, Y. and Huang, R.Z. (1997), "Determination of rock fracture toughness and its relationship with acoustic velocity", *Int. J. Rock Mech. Min. Sci.*, **34**(3), 49.e1-e11.

Chen, Z., Bunger, A.P., Zhang, X. and Jeffrey, R.G. (2009), "Cohesive zone finite element-based modeling of hydraulic fractures", *Acta Mechanica Solida Sinica*, **22**(5), 443-452.

Chen, W.Z., Wu, G.J. and Jia, S. (2010), *The Application of ABAQUS in Tunnel and Underground Engineering*, China Waterpower Press.

Cheng, Y. (2009), Boundary Element Analysis of the Stress Distribution Around Multiple Fractures: Implications for the Spacing of Perforation Clusters of Hydraulically Fractured Horizontal Wells, *Society of Petroleum Engineers*.

Gu, H. and Weng, X. (2010), "Criterion for fractures crossing frictional interfaces at non-orthogonal angles", *Proceedings of the 44th US Rock Mechanics Symposium and 5th US-Canada Rock Mechanics Symposium, American Rock Mechanics Association*.

He, M. and Hutchinson, J.W. (1989), "Kinking of a crack out of an interface", *J. Appl. Mech.*, **56**(2), 270-278.

Olson, J.E. and Wu, K. (2012), *Sequential vs. Simultaneous Multizone Fracturing in Horizontal Wells*:

Insights From a Non-Planar, *Multifrac Numerical Model*, Society of Petroleum Engineers.
Palmer, I.D. (1993), "Induced stresses due to propped hydraulic fracture in coalbed methane wells", *Low Permeability Reservoirs Symposium*, Denver, CO, USA, April.
Renshaw, C.E. and Pollard, D.D. (1995), "An experimentally verified criterion for propagation across unbounded frictional interfaces in brittle, linear elastic materials", *Int*. *J*. *Rock Mech*. *Min*. *Sci*. *Geomech*. *Abstracts*, **32**(3), 237-249.
Saberhosseini, S.E., Keshavarzi, R. and Ahangari, K. (2014), "A new geomechanical approach to investigate the role of in-situ stresses and pore pressure on hydraulic fracture pressure profile in vertical and horizontal oil wells", *Geomech*. *Eng*., *Int*. *J*., **7**(3), 233-246.
Shin, D.H. and Sharma, M.M. (2014), "Factors controlling the simultaneous propagation of multiple competing fractures in a horizontal well", *SPE Hydraulic Fracturing Technology Conference*, The Woodlands, TX, USA, Feburary.
Sneddon, I. (1946), "The distribution of stress in the neighbourhood of a crack in an elastic solid", *Proceedings of the Royal Society of London*. *Series A*. *Mathematical and Physical Sciences*, **187**(1009), 229-260.
Sneddon, I.N. and Elliot, H.A. (1946), "The opening of a Griffith crack under internal pressure", *Quart*. *Appl*. *Math*, **4**(3), 262-267.
Soliman, M.Y., East, L.E. and Augustine, J.R. (2010), "Fracturing design aimed at enhancing fracture complexity", *SPE EUROPEC/EAGE Annual Conference and Exhibition*, Barcelona, Spain, June.
Warpinski, N.R. and Branagan, P.T. (1989), "Altered-stress fracturing", *J*. *Petrol*. *Technol*., **41**(9), 990-997.
Warpinski, N.R. and Teufel, L.W. (1987), "Influence of geologic discontinuities on hydraulic fracture propagation (includes associated papers 17011 and 17074)", *J*. *Petrol*. *Technol*., **39**(2), 209-220.
Wu, H. and Chudnovsky, A., Dudley, J.W. and Wong, G.K. (2004), "A map of fracture behavior in the vicinity of an interface", *Gulf Rocks 2004 the 6th North America Rock Mechanics Symposium* (*NARMS*), Houston, TX, USA, June.
Yao, Y., Gosavi, S.V., Searles, K.H. and Ellison, T.K. (2010), "Cohesive fracture mechanics based analysis to model ductile rock fracture", *Proceedings of the 44th US Rock Mechanics Symposium and 5th US-Canada Rock Mechanics Symposium*, Salt Lake City, UT, USA, June.
Zhu, H.Y., Deng, J.G., Chen, Z.J., An, F.C., Liu, S.J., Peng, C.Y., Wen, M. and Dong, G. (2013), "Perforation optimization of hydraulic fracturing of oil and gas well", *Geomech*. *Eng*., *Int*. *J*., **5**(5), 463-483.
Zhu, H.Y., Deng, J.G., Zhao, J., Zhao, H., Liu, H.L. and Wang, T. (2014a), "Cementing failure of the casing-cement-rock interfaces during hydraulic fracturing", *Comput*. *Concrete*, *Int*. *J*., **14**(1), 91-107.
Zhu, H.Y., Deng, J.G., Liu, S.J., Wen, M., Peng, C.Y., Li, J.R., Chen, Z.J., Hu, L.B., Lin, H. and Dong, G. (2014b), "Hydraulic fracturing experiments of highly deviated well with oriented perforation technique", *Geomech*. *Eng*., *Int*. *J*., **6**(2), 153-172.

CC